Photoinduced dynamics of the valence states of ethene: A six-dimensional potential-energy surface of three electronic states with several conical intersections

Robert P. Krawczyk, Alexandra Viel, Uwe Manthe, Wolfgang Domcke

Photoinduced dynamics of the valence states of ethene: A six-dimensional potential-energy surface of three electronic states with several conical intersections

Robert P. Krawczyk, Alexandra Viel, Uwe Manthe, and Wolfgang Domcke
Institute of Physical and Theoretical Chemistry, Technical University of Munich, D-85747 Garching, Germany

(Received 10 February 2003; accepted 15 April 2003)

A six-dimensional analytic potential-energy surface of the three valence states (N, V, Z) of ethene has been constructed on the basis of complete-active-space *ab initio* calculations and *ab initio* calculations with perturbation theory of second order based on a complete active reference space. The nuclear coordinate space is spanned by the torsion, the C–C stretch coordinate, the left and right pyramidalization and the symmetric and antisymmetric scissor coordinates. The C–H stretch coordinates and the CH_2 rocking angles are kept frozen at their ground-state equilibrium value. A diabatic representation of the valence states of ethene has been constructed within the framework of a Hückel-type model. The diabatic potential-energy elements are represented as analytic functions of the relevant coordinates. The parameters of the analytic functions have been determined by a least-squares fit of the eigenvalues of the diabatic potential-energy matrix to the *ab initio* data for one-dimensional and two-dimensional cuts of the six-dimensional surface. As a function of the torsion, the analytic potential-energy surface describes the intersections of the V and Z states for torsional angles near 90°, which are converted into conical intersections by the antisymmetric scissor mode. As a function of pyramidalization of perpendicular ethene, it describes the intersections of the diabatic N and Z states, which are converted into conical intersections by displacements in the torsional mode. The analytic potential-energy surfaces can provide the basis for a quantum wave packet description of the internal conversion of photoexcited ethene to the electronic ground state via conical intersections. © *2003 American Institute of Physics.*
[DOI: 10.1063/1.1580092]

I. INTRODUCTION

Although the ethene molecule is absolutely fundamental both for organic photochemistry as well as electronic-structure theory, our understanding of the spectroscopy and photochemistry of ethene is far from complete.[1] Despite decades of spectroscopic investigations and electronic-structure calculations, there remain unsolved problems concerning the assignment of the UV absorption spectrum as well as the elementary reaction mechanisms of the photochemistry (for reviews, see Refs. 2–4).

The assignment of the UV absorption spectrum of ethene has turned out to be unexpectedly difficult. The reasons are the inherent diffuseness of the bands, preventing the application of high-resolution spectroscopy, the severe overlapping of intravalence and valence-Rydberg transitions, as well as the complete absence of fluorescence.[2–4] The spectrum of the intravalence $\pi\pi^*$ transition is an extremely extended quasi-continuum, exhibiting only faint indications of diffuse and partly irregular vibrational structure. The $\pi\pi^*$ spectrum is believed to have its intensity maximum at 61 700 cm^{-1} (7.65 eV).[3] The determination of its precise location is difficult because of overlapping transitions to Rydberg states. Although the electronic origin of the $\pi\pi^*$ transition cannot be directly observed due to its extremely low intensity (estimated as 10^{-12} of the intensity maximum[5]), it has been extrapolated to 5.5 eV.[6] The assignment of the weak and partly irregular vibrational structure with a spacing of about 800 cm^{-1} in C_2H_4 has been discussed controversially since the early investigations of Merer and Mulliken,[7] Foo and Innes,[6] and McDiarmid and Charney.[8] Wilkinson and Mulliken[5] and Merer and Mulliken,[7] for example, assigned the vibrational structure of the $\pi\pi^*$ spectrum to a progression in the C–C stretching vibration, while McDiarmid and Charney[8] assigned the structure as pure torsion. Activity in the symmetric scissoring and out-of-plane wagging modes has been observed in the UV resonance-Raman (RR) spectrum of ethene.[9] Overall, at least half a dozen of different assignments of the vibrational structure of the $\pi\pi^*$ transition have been discussed.[3]

The assignment of the transitions to the expected $3s$, $3p$, and $3d$ Rydberg states also has been found to be a surprisingly difficult task. The original assignment of the first Rydberg transition to $\pi\rightarrow 3s$ (Refs. 2–4) has later been called into question on grounds of both experimental observations[10] as well theoretical calculations,[10–12] which suggest the assignment of this band to the $\pi\rightarrow 3p_y$ transition.

Very recently, new spectroscopic information has been obtained by femtosecond pump–probe spectroscopy in the region of 6 eV (200 nm).[13,14] The time constant for internal conversion from the $^1\pi\pi^*$ state to the ground state has been determined as 30 ± 15 fs (Ref. 13) and 20 ± 10 fs (Ref. 14).

The interpretation of these data is not straightforward, however, since both electronic decay as well as irreversible motion of the initially prepared wave packet out of the ionization region may contribute to the observed decay of the pump–probe signal.[13,14]

The basic molecular-orbital (MO) model of ethene and a qualitative description of the PE functions of the electronic states has been developed by Mulliken[15] and discussed extensively in textbooks of organic photochemistry, see, e.g., Refs. 16–18. Following the convention of Mulliken, the electronic ground state and the valence excited singlet states are designed as N (for normal), V (for valence), and Z (for zwitterionic). Simple MO considerations indicate that the V state should exhibit a lengthened C–C bond and that the two CH_2 groups should be twisted by 90° at equilibrium (D_{2d} symmetry).[2] The doubly excited state (Z) is even more strongly stabilized by twisting and becomes nearly degenerate with the V state for torsional angles near 90°. Because of the quasidegeneracy of V and Z in twisted ethene, even a small one-sided pyramidalization results in a localization of the orbitals and in a zwitterionic structure (the so-called sudden-polarization effect).[16,19,20]

The calculation of the vertical electronic spectrum of ethene (D_{2h} symmetry) remains a challenge even for modern advanced electronic-structure theory. The reason is the quasidegeneracy of valence and Rydberg states discussed above. A balanced description of the compact valence states and the diffuse Rydberg states and their interaction requires extended basis sets and a very accurate treatment of electron correlation.[21–33] The degree of diffuseness of the electron density of the V state (measured by $\langle x^2 \rangle$) has been found to be a property of key importance for the calculation of the vertical excitation energy.[31–36] Since the accurate calculation of the vertical excitation energies is not the primary goal of the present work, we refer to the recent extensive studies of Krebs and Buenker[31] and Lischka and co-workers[33] for a more detailed discussion of this topic.

Pioneering calculations of the PE surfaces of the N, V, and Z states have been performed by Buenker *et al.*[20] and Persico and Bonačić-Koutecký[37] using the MRD-CI method. These calculations were focused on the torsional coordinate, the crossings of V and Z PE functions for torsional angles near 90°, and the sudden-polarization effect, as well as on crossings of the V state with the $3p$ Rydberg states.[11,12] One-dimensional torsional PE functions of the N, V, Z states have also been determined by Persico[38] and Dormans *et al.*[39] More recently, three-dimensional PE surfaces have been obtained by Groenenboom at the multireference CEPA level as a function of torsion, C–C stretch, and the symmetric scissors coordinate.[12] Ben-Nun and Martínez[1] and Molina *et al.*[40] have characterized in more detail the conical intersections between the N, V, and Z states with the MRCI and CASPT2 method, respectively. Additional nuclear degrees of freedom (hydrogen migration and hydrogen detachment) have been considered by Ohmine[41] and Evleth and Sevin.[42] The geometry of the minimum of the intersection seam of the S_1 and S_0 PE surfaces of ethene has been determined by Freund and Klessinger at the CASSCF level.[43]

An early calculation of the vibrational structure of the V state absorption spectrum has been performed by Warshel and Karplus within the Born–Oppenheimer, Condon, and harmonic approximations.[44] This approach has recently been further elaborated and combined with modern electronic-structure theory by Mebel *et al.*[30,45,46] The nonadiabatic coupling of the V state with some of the Rydberg states and the effect of this coupling on the vibronic structure of the UV absorption spectrum has been analyzed by several investigators.[10–12,46,47] Absorption spectra of nonadiabatically coupled V and Rydberg states have been calculated with the inclusion of one,[11] two,[10] and three vibrational modes,[12,47] resulting in conflicting assignments of the vibronic structure. These vibronic-structure calculations did not take into account the strong nonadiabatic coupling of the V state via the Z state with the electronic ground state ($V-Z$ and $Z-N$ conical intersections[1,40,43]). It should be mentioned that RR spectra of the V state[9,10] have been simulated by Siebrand, Zgierski and co-workers within three-dimensional models.[48,49]

The first time-dependent wave packet studies of the photochemistry of ethene have been performed by Persico[38] and Dormans *et al.*[39] within one-dimensional models (torsion only). It is clear from the above-discussed electronic-structure calculations on the qualitative shape of the PE surfaces of ethene that at least the torsion, the C–C stretch motion, and the pyramidalization have to be included in the description of the photochemical dynamics. Possibly also the symmetric scissoring motion[47–49] and hydrogen migration[41] are involved. The construction of *ab initio* PE surfaces which are appropriate for time-dependent wave packet simulations of the photochemical dynamics of ethene, in particular, the internal conversion to the electronic ground state, thus is a challenging task, which has not been tackled so far. The difficulty of this task is considerably enhanced by the existence of several conical intersections. As a consequence, a reasonably efficient interpolation of the *ab initio* PE surfaces requires the construction of a diabatic representation of the electronic states (see Refs. 50–53 for reviews).

An alternative approach, which bypasses the bottleneck of the construction of multisheeted multidimensional PE surfaces, is based on so-called direct-dynamics methods, see, e.g., Refs. 54–57. *Ab initio* direct-dynamics simulations of the photochemistry of ethene have been recently been performed by Ben-Nun and Martínez, employing the so-called multiple-spawning method within a minimal-active-space CASSCF framework.[56,58] Granucci *et al.* have performed direct-dynamics simulations of the photochemistry, using the surface-hopping method[59] within a semiempirical model of the electronic structure of ethene.[60] While these direct-dynamics calculations are full-dimensional, they are, at least for the foreseeable future, limited to rather crude electronic-structure models and involve an approximate treatment of the nonadiabatic dynamics (surface hopping,[59] Ehrenfest mean-field dynamics,[61] or variants thereof). The simulations of Ben-Nun and Martínez and Granucci *et al.* yield different values for the lifetime of the V state [180 fs (Ref. 56) and 50 fs (Ref. 60), respectively], which may be the consequence of the different electronic-structure models or the different approximations in the treatment of the nonadiabatic dynamics.

The multiple-spawning direct-dynamics method also has been applied to the calculation of UV absorption and RR spectra of ethene, although with limited success.[62] The approximations involved appear to be too crude to allow predictive calculations of the complex vibronic structure of the UV absorption spectrum or RR excitation profiles of ethene.

The aim of the present work is the construction of multidimensional PE surfaces of the ground and intravalence excited states of ethene, which significantly goes beyond previous attempts. We focus on the singlet valence states (N, V, Z), because these play the essential role in the internal-conversion dynamics of photoexcited ethene, which we want to understand in microscopic detail. The consideration of the excited states of Rydberg character and their nonadiabatic coupling with the V state certainly is important for the description of the UV and RR spectra. These aspects have to be considered in future extensions of the present model of the valence-state photochemistry.

It appears impossible to develop from the outset a full-dimensional multistate PE surface of ethene in a systematic manner. We have decided to take into account six of the twelve internal coordinates in the construction of the surface. These include the torsion, the C–C stretch coordinate, and the left and right pyramidalization, which have been known to play a prominent role in the spectroscopy and photochemistry, as discussed above. We have found that, in addition, the inclusion of the antisymmetric scissoring motion is absolutely essential, since it is this mode which couples the quasidegenerate V and Z states in D_{2d} symmetry in first order. For completeness, the symmetric scissoring coordinate also is included, resulting in a six-dimensional nuclear coordinate space (torsion, C–C stretch, two pyramidalizations, two scissors). The C–H stretch coordinates, on the other hand, as well as the symmetric and antisymmetric rocking coordinates, are kept frozen. It is well established that C–H stretch motions are essentially Franck–Condon inactive in the $N \rightarrow V$ transition.[2–4] Nevertheless, as pointed out in,[41,43,56] hydrogen migration may come into play at later stages of the photoinduced dynamics. Moreover the high-frequency C–H-stretch modes may contribute, via anharmonic stretch–bend coupling on the ground-state PE surface, as accepting modes to the internal-conversion process. It should be kept in mind that these effects are not included in the present PE model.

We have adopted the CASSCF/CASPT2 electronic-structure model[63,64] as a compromise between accuracy and computational cost. Although highly accurate MCSCF/MRCI calculations with extended basis sets are technically feasible for the excited states of ethene (see, e.g., Ref. 33), these calculations are too expensive for the scanning of large parts of even few-dimensional surfaces. For a relatively small molecule like ethene, the nondynamical electron-correlation effects can quite efficiently be treated at the CASSCF level. The remaining correlation effects, which are of dynamical character, are then reasonably accurately recovered by the CASPT2 method. Compared with the direct-dynamics approach, we can employ larger basis sets and much better tailored active spaces. The diabatization of the two conical intersections is achieved with the help of a qualitative electronic-structure model of the Hückel-type, the parameters of which are determined via a least-squares fitting of the eigenvalues of the 3×3 PE matrix to the *ab initio* data.

II. ELECTRONIC-STRUCTURE METHODS

As a reference for the definition of the internal displacement coordinates, the ground-state equilibrium geometry has been determined. The ground-state equilibrium geometry and the harmonic frequencies were computed by the MP2 method using GAUSSIAN 98.[65] For these calculations Dunning's cc-pVTZ basis[66] set was used.

The *ab initio* calculations of the ground and excited state PE surfaces have been performed at the CASSCF and CASPT2 levels, employing the cc-pVTZ basis set. The choice of this rather compact basis set is justified, because we are primarily interested in the intravalence excited states in regions of nuclear coordinate space where valence-Rydberg mixing is not important. For the CASSCF calculations, an active space of ten electrons distributed over ten orbitals has been chosen. A full-valence CAS would consist of twelve active electrons distributed over twelve active orbitals. Since the calculations had to be performed without symmetry restrictions on the electronic wave functions to avoid artefactual symmetry-breaking effects, 12/12-CASSCF calculations are quite time-consuming. We have checked by test calculations that a 10/10 CASSCF (excluding the $2s$ carbon orbitals from the active space) is a good approximation to a full-valence CASSCF for the electronic states of interest in the relevant regions of the nuclear coordinate space.

To achieve a balanced description of the ground and excited electronic states, the three lowest electronic states have been included in the CASSCF energy functional with equal weights.

The calculation of cuts of the PE surfaces along the torsional coordinate, which plays the role of the dominant large-amplitude nuclear motion, has been initiated at a torsional angle φ of 90° (D_{2d} symmetry for nonpyramidalized ethene). At this geometry, mixing of the valence states with Rydberg states is irrelevant, since the valence states are much lower in energy than the Rydberg states. In order to follow the valence excited states towards the planar configuration (D_{2h} symmetry), the CASSCF orbitals of the previous geometry (with larger torsional angle) have been employed as starting orbitals for the wave function optimization.

At the ground-state equilibrium geometry, the V and Z states are embedded in a manifold of Rydberg states. With the present basis set, the Z state is the sixth excited state at this geometry. Converged calculations for the six lowest states would be very difficult to perform. Therefore the PE of the Z state has not been calculated for near-planar geometries. This part of the PE surface of the Z state is irrelevant for the photochemistry initiated by the excitation of the V state.

The inclusion of dynamical correlation effects is indispensable to obtain PE surfaces which are of sufficient accuracy for the study of spectroscopic and photochemical phenomena. The dynamical correlation energy has been

TABLE I. Ground-state harmonic frequencies of ethene (in cm^{-1}).

Symmetry	Mode	Frequency MP2 (this work)	CCSD(T)[a]	Expt.[b]	Description
a_g	ν_1	3196	3157	3156	C–H sym. stretch
	ν_2	1684	1672	1656	C–C stretch
	ν_3	1384	1369	1372	CH_2 sym. scissor
a_u	ν_4	1076	1044	1045	torsion
b_{1u}	ν_5	3178	3139	3130	C–H sym. stretch
	ν_6	1485	1479	1472	CH_2 antisym. scissor
b_{2g}	ν_7	960	942	960	CH_2 pyramid. (wagging)
b_{2u}	ν_8	3293	3246	3239	C–H antisym. stretch
	ν_9	828	823	844	CH_2 sym. rocking
b_{3g}	ν_{10}	3266	3219	3207	C–H antisym. stretch
	ν_{11}	1247	1242	1249	CH_2 antisym. rocking
b_{3u}	ν_{12}	984	967	968	CH_2 pyramid. (wagging)

[a]Reference 71.
[b]Reference 74.

determined with the CASPT2 method.[64] The multistate version of CASPT2 (MS-CASPT2) (Ref. 67) has been employed. Single-state CASPT2 calculations have been performed for comparison. For most parts of the PE surface, the MS-CASPT2 and single-state CASPT2 results are essentially identical. A level shift of 0.3 a.u. has been found to be appropriate for the minimization of intruder-state problems. All CASSCF and CASPT2 calculations have been performed with the MOLCAS-5 program package.[68]

The calculation of the PES on a grid in six dimensions is not feasible. Our approach to the construction of a qualitatively useful PE surface of ethene is based on the calculation of one-dimensional and two-dimensional cuts. One-dimensional cuts have been calculated along the six selected coordinates (torsion, C–C stretch, two pyramidalizations, two scissors) to obtain an overview of important features of the surface. Then two-dimensional cuts were computed, to take account of the nonseparability of the vibrational modes in a pairwise manner. Not all possible pairs of the six selected coordinates have been taken into account. Since the torsion breaks the C–C double bond, it has a pronounced effect on the shape of the PE surfaces in the other coordinates. Therefore, two-dimensional cuts of the torsion with the other five coordinates were included in the construction of the surface.

The definition of the C–C distance, r, is obvious. The torsional angle, φ, is defined as the angle between the two vectors connecting the hydrogen atoms of the CH_2 groups. The one-sided pyramidalization is defined as the angle of the vector from the carbon atom to the center of the two hydrogen atoms with the axis through the two carbon atoms. The left(right) pyramidalization are denoted as ϑ_l and ϑ_r, respectively. The scissoring displacement coordinates were defined as symmetric and antisymmetric linear combinations,

$$\alpha_a = \frac{\alpha_r - \alpha_l}{2}, \tag{1a}$$

$$\alpha_s = \frac{(\alpha_r - \alpha_0) + (\alpha_l - \alpha_0)}{2}, \tag{1b}$$

where α_l and α_r are the left and right scissor angles, respectively, and α_0 is the scissor angle at the ground-state equilibrium geometry.

As a function of the torsional angle, the energies have been calculated on an equidistant grid from $\varphi = 0$ to $\varphi = 90°$ in steps of 10°. A much denser grid has been chosen for $\varphi > 70°$, where the V and Z states become close in energy and interact via other vibrational modes. The pyramidalization angle has been varied between $\vartheta = 0$ and $\vartheta = 150°$ in steps of 10°. As a function of the symmetric and antisymmetric scissoring coordinates, the energies were calculated between $-30°$ and 30° with a step size of 2°. The C–C distance r has been varied between 1.132 and 1.732 Å in steps of 0.1 Å. In several critical regions of the PE surface, a higher density of the grid points has been chosen.

A technical problem has been encountered in the calculations involving displacements in the antisymmetric scissor coordinate near $\varphi = 90°$. The α_a coordinate couples the nearly degenerate V and Z states of perpendicular ethene in first order. The resulting strong mixing of the electronic states for small, but nonzero, α_a cannot properly be described with either the single-state CASPT2 method or MS-CASPT2. The vibronic interaction is, on the other hand, properly (and presumably also with good accuracy) described at the CASSCF level. The one-dimensional and two-dimensional cuts involving the antisymmetric scissoring mode were therefore calculated with the CASSCF method.

III. ADIABATIC POTENTIAL-ENERGY SURFACES

A. Ground-state equilibrium geometry and vertical excitation energies

The optimization of the ground-state geometry of ethene yields a C–C distance of 1.332 Å, a C–H distance of 1.081 Å, and a HCH angle of 117.3°. These values have an error which is less then one percent in comparison to the experimental data.[69,70] This optimized geometry was used as the reference geometry for all calculations performed at the MS-CASPT2 level of theory.

In Table I the ground-state harmonic vibrational frequen-

TABLE II. Calculated excitation energies (in eV) of the N, V, and Z states at $\varphi=0$ and $\varphi=\pi/2$.

State	$\varphi=0$	$\varphi=\pi/2$
N	⋯	3.06
		2.8[a]
V	7.95	5.48
	8.07,[a] 7.69,[b] 8.40[c]	5.4,[a] 6.29[i]
	7.99,[d] 7.98,[e] 7.99[f]	
	7.96,[g] 7.90–7.95[h]	
Z		5.38
	$\approx$12.5[i]	5.4,[a] 6.15[i]

[a]MSPT2 (Ref. 40).
[b]MRCI-AQCC (Ref. 33).
[c]CASPT2 (Ref. 28).
[d]EOM-CCSD(T) (Ref. 29).
[e]MS-CASPT2 (Ref. 67).
[f]CAS-SDCI (Ref. 32).
[g]MRCI (Ref. 21).
[h]MRD-CI (Ref. 31).
[i]MRD-CI (Ref. 20).

cies of ethene are summarized. Compared to other calculations[71,72] or spectroscopic data,[9,73] the error of the MP2 harmonic frequencies is less than 2%.

At the ground-state equilibrium geometry, single-point CASSCF and MS-CASPT2 calculations have been performed to determine the vertical excitation energies. The first excited singlet state is the $\pi\pi^*$ excited state, and the second excited state at this geometry is the 3s Rydberg state. The vertical excitation energy of the V state is found to be 7.95 eV and is compared in Table II with other calculations from the literature. It can be seen that the calculated excitation energies of the V state lie between about 7.6 eV and 8.4 eV. The currently best value is 7.69 eV, estimated by Müller *et al.* from large MR-AQCC and MR-SDCI calculations.[33] The latter value is in good agreement with the estimated maximum of the $\pi\pi^*$ absorption band.[11] It should be stressed that our calculations have been tailored to yield global valence-state PE surfaces; neither the basis set nor the active space have been optimized to give good vertical excitation energies.

The present calculation gives a value of $12.7a_0^2$ for $\langle x^2\rangle$, which is, as expected for the cc-pVTZ basis set, too low in comparison with the currently best estimate of about $17a_0^2$.[33] As found in previous CASPT2 calculations, the vertical excitation energy of the V state is slightly overestimated by the CASPT2 method.[28,35,67]

Theoretical data for the excitation energies at $\varphi=\pi/2$, with all other coordinates fixed at their ground-state equilibrium value, are much more scarce. At this geometry, we find an excitation energy for the V state of 5.48 eV and an excitation energy of 5.38 eV for the Z state. In agreement with Buenker *et al.*,[20] the Z state is the lowest excited state at $\varphi=\pi/2$. Molina *et al.*[40] have assumed in their MS-CASPT2 calculations that at $\varphi=\pi/2$ the V and Z state are truly degenerate states. But symmetry rules this possibility out, since the electrons occupy e-orbitals, and $e\otimes e$ contains only one-dimensional representations in D_{2d} symmetry. Therefore only an accidental degeneracy is possible. Our calculated excitation energy of the V state of perpendicular ethene is in good agreement with the extrapolated origin of the V state absorption band of about 5.5 eV.[6]

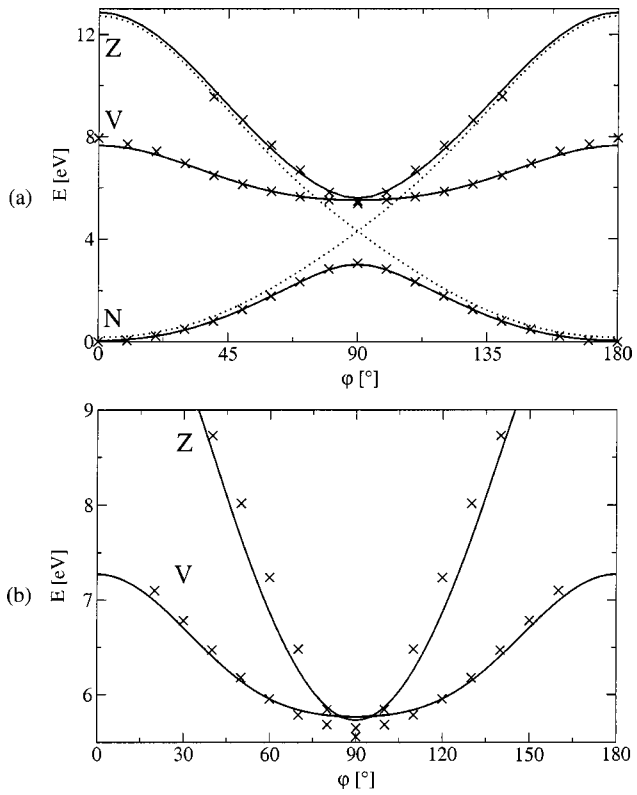

FIG. 1. Analytic global fit (full lines) and *ab initio* points (crosses) of the adiabatic PEs of the N, V, and Z states along φ (for $\vartheta=0$) at (a) the ground-state equilibrium C–C distance and at (b) 1.486 Å, the equilibrium value of the V state, optimized in D_{2h} symmetry (Ref. 1). In (b) only the two excited adiabatic states (V, Z) are shown. The diabatic potentials are displayed as dotted lines in (a).

The barrier height for rigid torsion in the ground state is found to be 3.06 eV. At the perpendicular geometry, the ground state and the first excited state (Z) are separated by 2.32 eV. In comparison with the MS-CASPT2 calculations of Molina *et al.*[40] and the SA-6-CAS(2/6)*SDCI results of Ben-Nun *et al.*,[1] which both found an energy gap of about 2.5 eV, this value appears to be too low. The deviation may be due to the different basis sets used or the different active spaces.

B. One-dimensional cuts

For the photophysics of ethene, the most important one-dimensional cut is along the torsion. The torsional potential-energy functions are presented in Fig. 1 for two different C–C distances, the equilibrium r value of the ground state [Fig. 1(a)] and $r=1.486$ Å, which is the equilibrium r value of the V state in D_{2h} symmetry[1] [Fig. 1(b)]. Here and in the following, all energies are referred to the minimum energy of the electronic ground-state. As already found by Buenker *et al.*[20] and Ohmine,[41] the V and Z states cross between $\varphi=80°$ and $\varphi=90°$, when r is kept fixed at the ground-state equilibrium value. An inspection of the wave function at the D_{2d} geometry reveals that the singly excited state (V) is the second excited state at this geometry.

The crossing of the V and Z states along the torsion gives rise to two pairs of conical intersections. For these

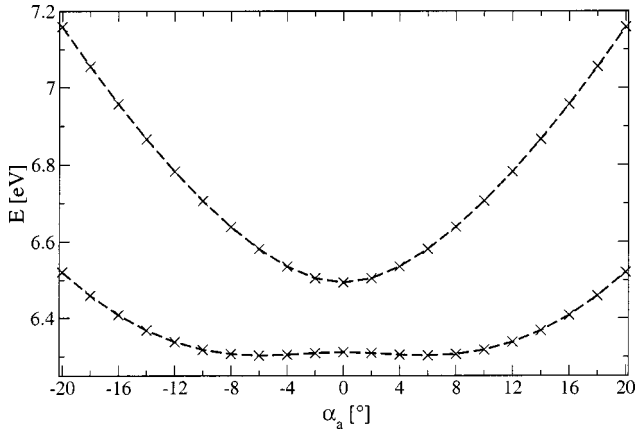

FIG. 2. Adiabatic PE functions of the Z and V states along α_a at $\varphi = \pi/2$, calculated at the CASSCF level. The dashed lines connect the *ab initio* data (crosses).

intersections, the torsion is the tuning mode leading to the intersection, and the antisymmetric scissor mode is the coupling mode, leading to vibronic coupling in first order. The conical intersection between the two excited states is located between $\varphi = 80°$ and $\varphi = 90°$. Buenker *et al.* have located the conical intersection at $\varphi = 82°$.[20]

In Fig. 2, the one-dimensional cut calculated at the CASSCF level along α_a at $\varphi = \pi/2$ is shown. The cut at the perpendicular geometry was chosen, because the coupling between the two excited states and the ground state is at a minimum at this geometry. The double-minimum shape of the lower (Z state) PE function is characteristic for linear vibronic coupling by a nontotally symmetric mode.[75,76]

In twisted ethene, the nearly degenerate V and Z states also interact via the pyramidalization coordinate (the sudden-polarization effect[19,20]). A symmetry analysis reveals that this coupling is in second order in the pyramidalization. The PE functions along ϑ (one-sided pyramidalization) of perpendicular ethene are shown in Fig. 3. It is seen that the Z state is stabilized by pyramidalization and intersects the N state for $\vartheta \approx 115°$. This intersection has been discussed previously in Refs. 1, 40, and 42.

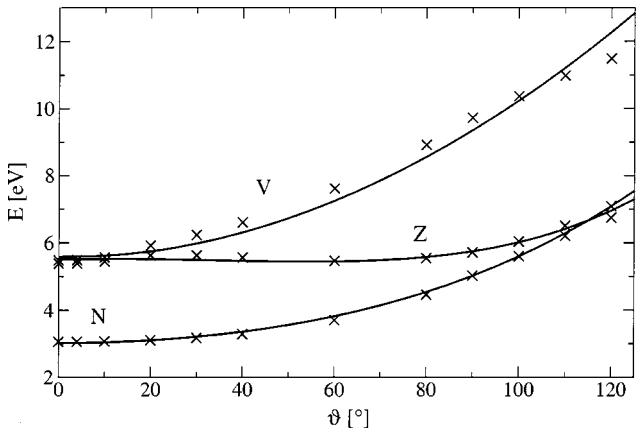

FIG. 3. Adiabatic PEs of the valence states of perpendicular ethene ($r = 1.332$ Å) as a function of the one-sided pyramidalization angle ϑ. Crosses: *ab initio* data; full lines: global analytic fit (see text).

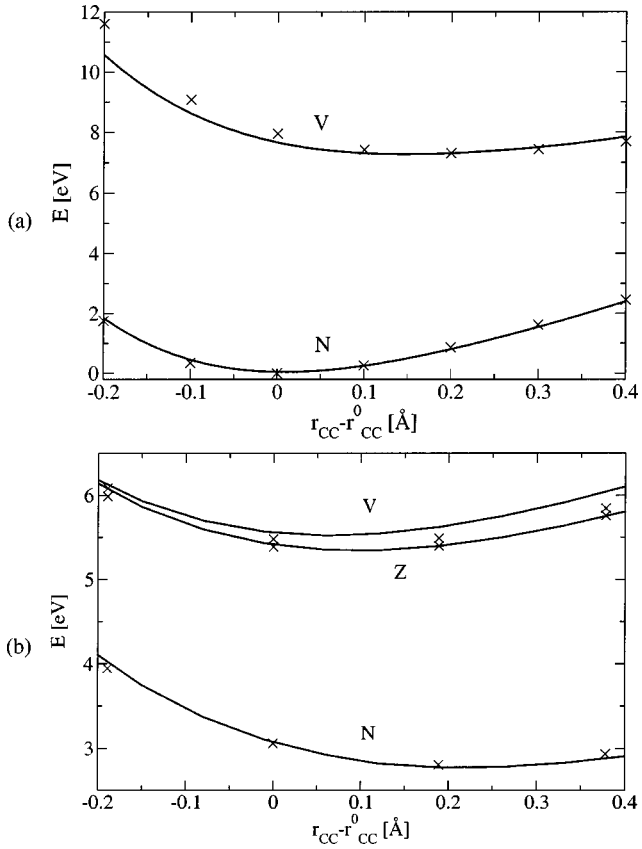

FIG. 4. Adiabatic PEs of the valence states of planar (a) and perpendicular (b) ethene as a function of the C–C distance. Crosses: *ab initio* data. Full lines: global analytic fit (see text).

The adiabatic PES of the N, V, and Z states as a function of the C–C stretch coordinate are shown in Fig. 4 for (a) planar and (b) perpendicular ethene. The Z state PE function is not included in (a), because it is too high in energy. One can see that the V-state PE minimum along this cut is located at $r \approx 1.52$ Å in planar ethene and at $r \approx 1.38$ Å in perpendicular ethene. These results are in good agreement with the MS-CASPT2 geometry optimizations of Molina *et al.*[40]

In perpendicular ethene, Fig. 4(b), the minimum of the ground state occurs at much longer C–C distances, reflecting the missing π bond. The minimum of the V state along this cut is found at a C–C distance which is about 0.1 Å shorter than the minimum of the same cut for $\varphi = 0$.

C. Two-dimensional cuts

Contour plots of the adiabatic PE surfaces as a function of the torsion and the coordinates ϑ, r, and α_s are shown in Figs. 5–7. The *ab initio* data, interpolated by a cubic spline, are shown as the dotted lines. The full lines represent the global analytic fit to the *ab initio* data (see Sec. IV). The two-dimensional cut as a function of φ and α_a has been computed at the CASSCF level only, as explained in Sec. II. A cubic-spline interpolation of these data in the φ, α_a plane is shown in Fig. 8.

The most interesting surface is the two-dimensional surface along torsion and pyramidalization, which has been discussed previously.[56] A contour plot of the S_0, S_1, and S_2 *ab*

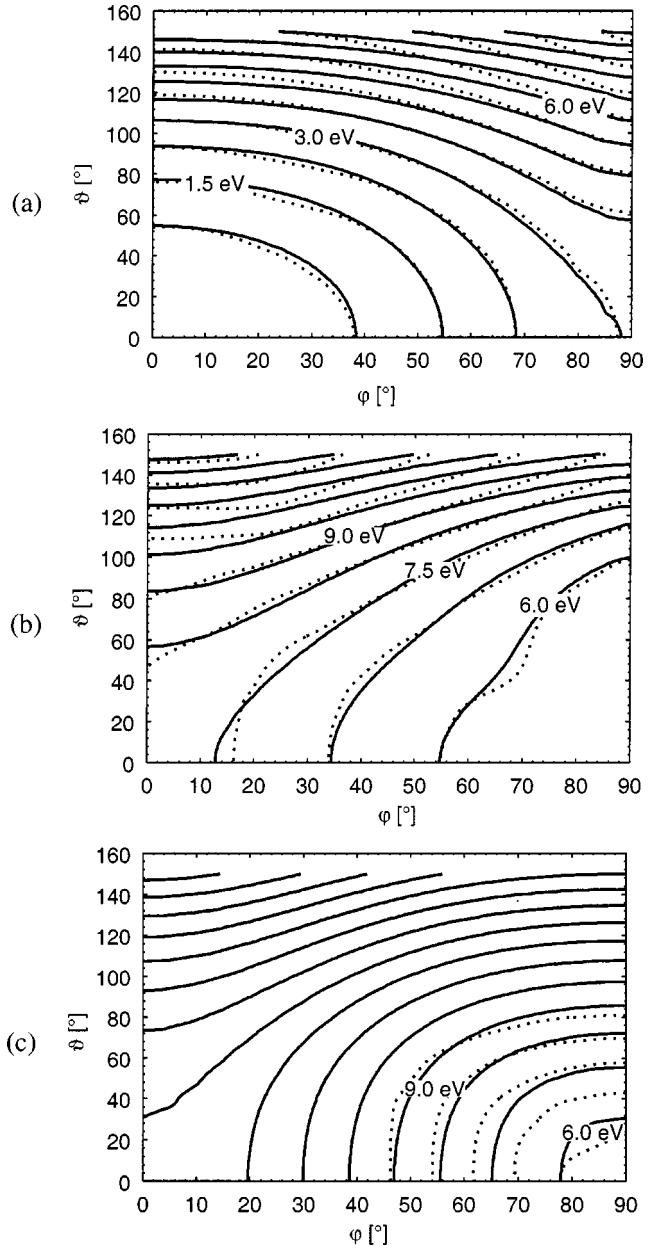

FIG. 5. Contour plots of the adiabatic PE surfaces as a function of φ and ϑ. A cubic spline interpolation of the *ab initio* data is shown as dotted lines, while the global analytic fit is given by the full lines. (a) Ground state, (b) first excited state, (c) second excited state. The contour lines have a spacing of (a)–(b): 0.75 eV, (c): 1.00 eV.

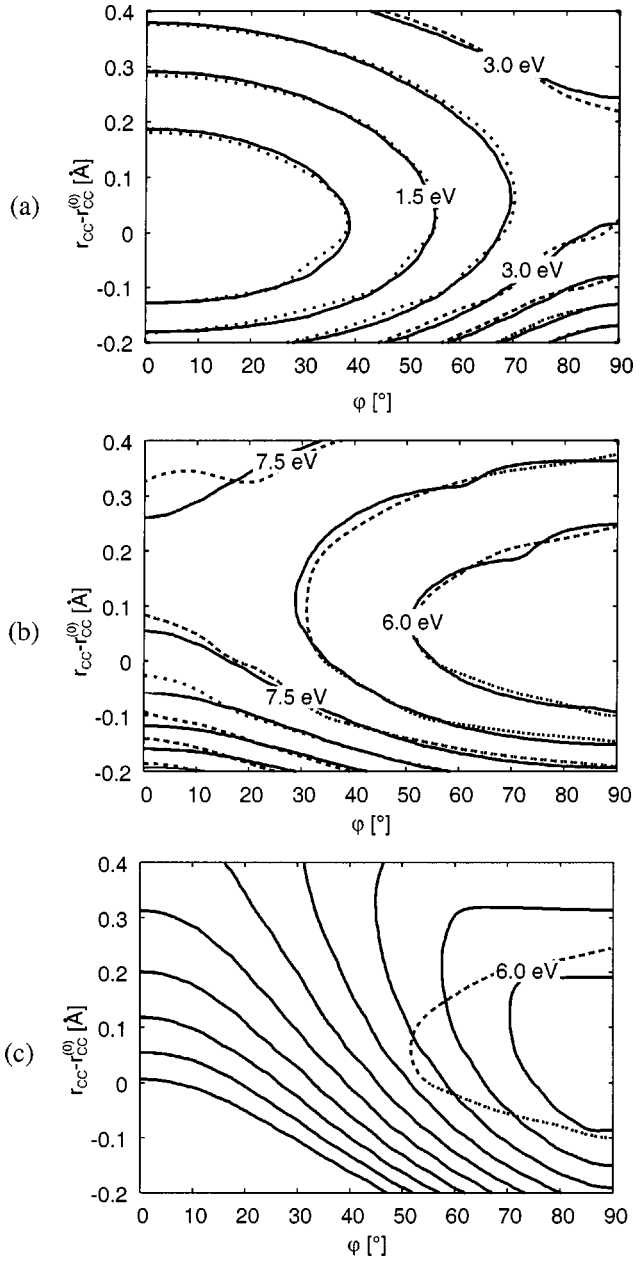

FIG. 6. Contour plots of the adiabatic PE surfaces as a function of φ and r. A cubic spline interpolation of the *ab initio* data is shown as dotted lines, while the global analytical fit is given by the full lines. (a) Ground state, (b) first excited state, (c) second excited state. The contour lines have a spacing of 0.75 eV.

initio surfaces is shown in Fig. 5. The PE surfaces of the ground state and first excited state can be computed with good quality over the complete range of φ and ϑ. The S_2 energies have been computed only for $\varphi > 40°$ to avoid perturbation of the data by crossings with Rydberg states. The S_0 and S_2 surfaces are very steep along ϑ, while the S_1 surface is more shallow for near-perpendicular geometries. The surfaces of Fig. 5 show a strong nonseparability of torsion and pyramidalization.

The effect of the C–C distance on the torsional potentials is revealed by Fig. 6. It can be seen that the torsion and C–C stretch mode are strongly coupled in the ground as well as excited states. The C–C equilibrium distance increases as a function of φ in the electronic ground state [Fig. 6(b)]. This reflects the breaking of the π bond upon torsion. In the V state, on the other hand, the C–C equilibrium distance decreases with increasing torsion, in agreement with simple MO considerations. The PE surface of the Z state has been calculated for $\varphi > 40°$ only and is thus incomplete. Because it is not of relevance of the UV photochemistry of ethene, no attempts have been made to generate a more extended Z-state surface.

In Fig. 7 the PE surfaces are shown as a function of φ and α_s. It is seen that the nonseparability of φ and α_s is rather weak. The equilibrium geometry as a function of α_s is almost independent of φ in both N and Z states.

The adiabatic PE surfaces as a function of φ and the

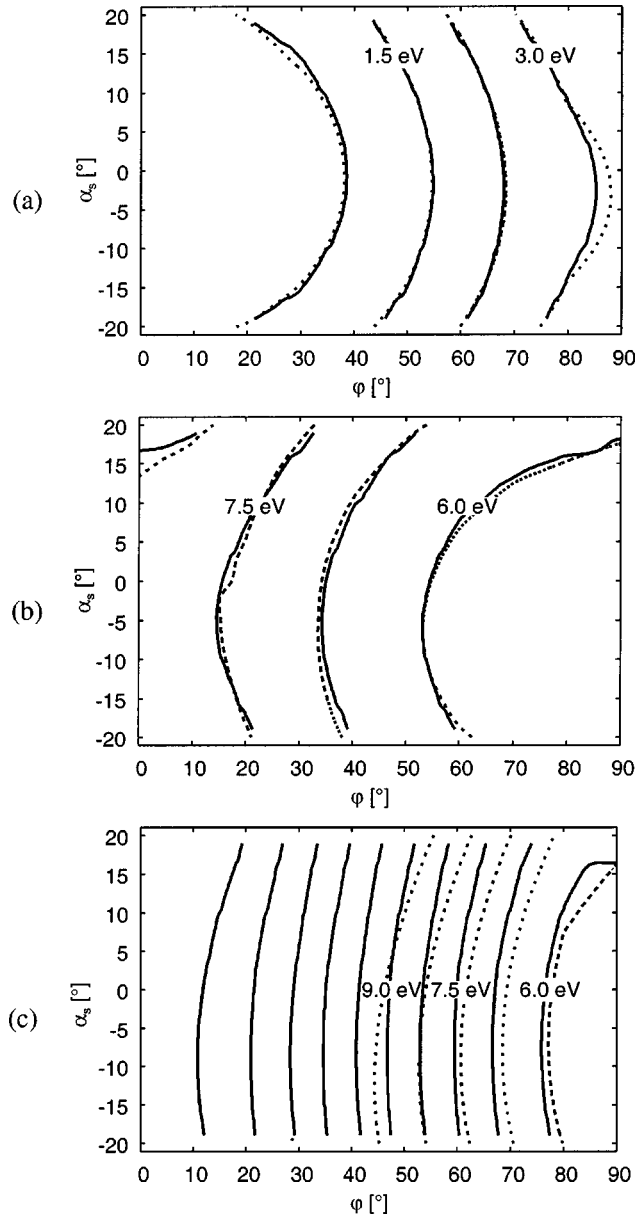

FIG. 7. Contour plots of the adiabatic PE surfaces as a function of φ and α_s. A cubic spline interpolation of the *ab initio* data is shown as dotted lines, while the global analytic fit is given by the full lines. (a) Ground state, (b) first excited state, (c) second excited state. The contour lines have a spacing of 0.75 eV.

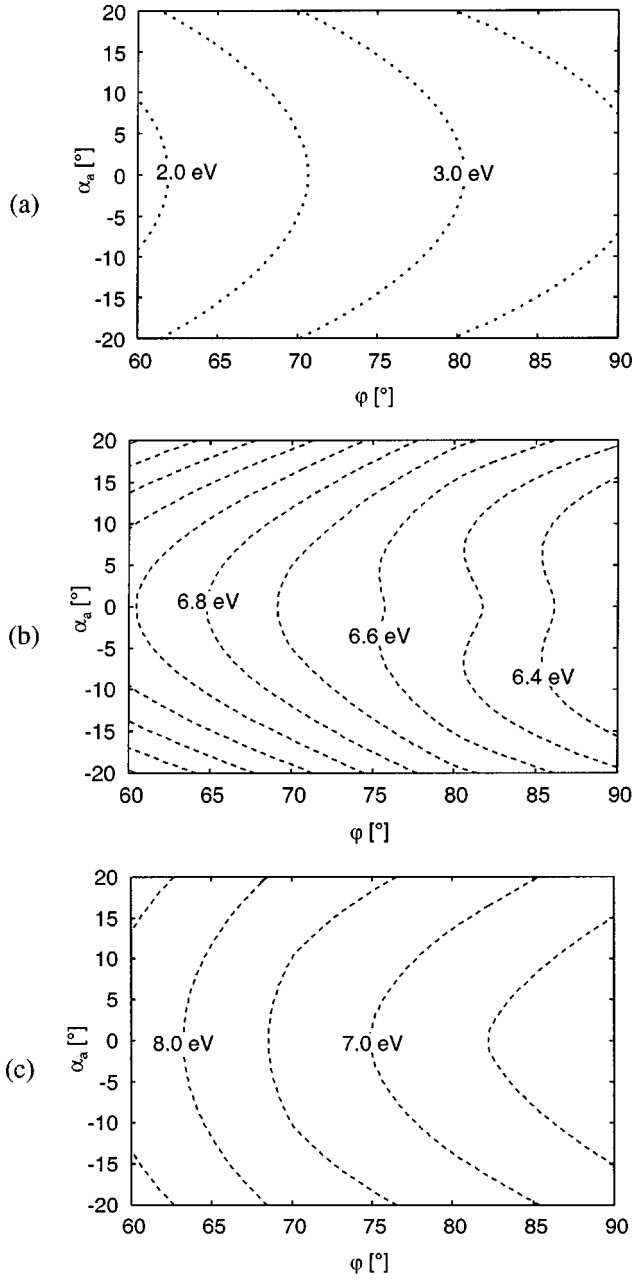

FIG. 8. Contour plots of the adiabatic PE surfaces as a function of φ and α_a. A cubic spline interpolation of the *ab initio* data (CASSCF) is shown as dotted lines. (a) Ground state, (b) first excited state, (c) second excited state. The line spacing for (a) and (c) is 0.5 eV, for (b) it is 0.1 eV.

antisymmetric scissor coordinate α_a, calculated at the CASSCF level, are displayed in Fig. 8. For the N and Z states, the PES are essentially separable in φ and α_a. In the adiabatic S_1 state, on the other hand, we observe the development of a double-minimum potential as a function α_a for large torsional angles ($\varphi > 75°$). This feature reflects the first-order vibronic coupling between the V and Z states via α_a for near-perpendicular geometries, as discussed above.

IV. DIABATIC POTENTIAL-ENERGY SURFACES AND GLOBAL ANALYTIC FIT

A. Electronic-structure model for the *N*, *V*, and *Z* states

Omitting the σ framework and considering only the $2p$ orbitals on the carbon atoms, the N state has the configuration π^2 and V corresponds to the singly excited state with the configuration $\pi\pi^*$. The Z state is the doubly excited state with a π^{*2} configuration.

The diabatic states can be constructed employing delocalized π/π^* orbitals. These are given as the symmetric and antisymmetric combinations of the $2p$ orbitals of the carbon atoms. This choice of MOs is very natural at the equilibrium geometry. However, torsion around the carbon–carbon axis plays a prominent role in the photoexcitation process. At a twisted geometry, corresponding to a 90° torsional angle, the overlap between the $2p$ orbitals vanishes. Instead of using the delocalized orbitals,

$$|\pi\rangle = \frac{1}{\sqrt{2}}(|2p_r\rangle + |2p_l\rangle), \tag{2a}$$

$$|\pi^*\rangle = \frac{1}{\sqrt{2}}(|2p_r\rangle - |2p_l\rangle), \tag{2b}$$

it might then be more convenient to use the localized orbitals,

$$|r\rangle = |2p_r\rangle, \tag{3a}$$

$$|l\rangle = |2p_l\rangle, \tag{3b}$$

directly. It should be pointed out that in Eq. (2) a vanishing overlap of the $|2p_r\rangle$ and $|2p_l\rangle$ orbitals has been assumed. Since Eqs. (2) and (3) are used here only to motivate a localized-to-delocalized transformation matrix, which is constructed in a geometry-independent manner, the overlap between the $|2p_r\rangle$ and $|2p_l\rangle$ orbitals needs not to be considered explicitly. A similar approach, which includes the overlap explicitly, has been formulated by Tennyson and Murrell.[77]

Using these orbitals, two alternative sets of diabatic states can be constructed. A delocalized description based on the states $|\pi^2\rangle$, $|\pi\pi^*\rangle$, and $|\pi^{*2}\rangle$ can be chosen, or a localized representation employing the states $|r^2\rangle$, $|rl\rangle$, and $|l^2\rangle$. Here $|\pi\pi^*\rangle$ and $|rl\rangle$ are to be understood as linear combinations which are properly antisymmetrized with respect to electron exchange.

The diabatic PE matrix in the delocalized basis is defined as

$$\mathbf{V} = \begin{pmatrix} V_{\pi^2} & V_{\pi^2,\pi^{*2}} & V_{\pi^2,\pi\pi^*} \\ V_{\pi^2,\pi^{*2}} & V_{\pi^{*2}} & V_{\pi^{*2},\pi\pi^*} \\ V_{\pi^2,\pi\pi^*} & V_{\pi^{*2},\pi\pi^*} & V_{\pi\pi^*} \end{pmatrix}. \tag{4}$$

Equivalently, the PE matrix can be written in the localized basis as

$$\mathbf{U}^\dagger\mathbf{V}\mathbf{U} = \begin{pmatrix} V_{r^2} & V_{r^2,l^2} & V_{r^2,rl} \\ V_{r^2,l^2} & V_{l^2} & V_{l^2,rl} \\ V_{r^2,rl} & V_{l^2,rl} & V_{rl} \end{pmatrix}, \tag{5}$$

where the transformation matrix is given by

$$\mathbf{U} = \begin{pmatrix} \frac{1}{2} & \frac{1}{2} & \frac{1}{\sqrt{2}} \\ \frac{1}{2} & \frac{1}{2} & -\frac{1}{\sqrt{2}} \\ \frac{1}{\sqrt{2}} & -\frac{1}{\sqrt{2}} & 0 \end{pmatrix}. \tag{6}$$

The above PE matrices can be characterized by six independent potential functions. Choosing definitions which treat the localized and delocalized representation symmetrically, we introduce the six functions $V_{\mathrm{pot}}, V_z, V_\pi, V_{\mathrm{pyr}}, V_c$, and V_Δ. Employing these functions, the diabatic matrix elements are written as

$$V_{\pi^2} = V_{\mathrm{pot}} + \frac{V_c}{2} + V_\pi, \tag{7a}$$

$$V_{\pi^{*2}} = V_{\mathrm{pot}} + \frac{V_c}{2} - V_\pi, \tag{7b}$$

$$V_{\pi\pi^*} = V_{\mathrm{pot}} - V_c, \tag{7c}$$

$$V_{\pi^2,\pi\pi^*} = \frac{1}{\sqrt{2}}(V_{\mathrm{pyr}} + V_z), \tag{7d}$$

$$V_{\pi^{*2},\pi\pi^*} = \frac{1}{\sqrt{2}}(V_{\mathrm{pyr}} - V_z), \tag{7e}$$

$$V_{\pi^2,\pi^{*2}} = V_\Delta + \frac{V_c}{2}, \tag{7f}$$

in the delocalized basis and

$$V_{r^2} = V_{\mathrm{pot}} + \frac{V_\Delta}{2} + V_{\mathrm{pyr}}, \tag{8a}$$

$$V_{l^2} = V_{\mathrm{pot}} + \frac{V_\Delta}{2} - V_{\mathrm{pyr}}, \tag{8b}$$

$$V_{rl} = V_{\mathrm{pot}} - V_\Delta, \tag{8c}$$

$$V_{r^2,rl} = \frac{1}{\sqrt{2}}(V_\pi + V_z), \tag{8d}$$

$$V_{l^2,rl} = \frac{1}{\sqrt{2}}(V_\pi - V_z), \tag{8e}$$

$$V_{r^2,l^2} = \frac{V_\Delta}{2} + V_c, \tag{8f}$$

in the localized basis.

The potential function V_{pot} always appears on the diagonal of $\mathbf{V}$, independent of the representation. Similarly, V_z keeps its off-diagonal position. These functions thus play the same role in the localized and delocalized representations. Therefore, they cannot be connected to any π-binding effects. They should therefore describe mainly σ-binding and steric effects. V_π and V_{pyr}, on the other hand, exchange their position when changing from the delocalized to the localized representation. Investigating the delocalized representation, V_π can obviously be associated with the π-binding energy. $2V_\pi$ is the energy difference between the $|\pi^2\rangle$ and $|\pi^{*2}\rangle$ states. Similarly, $2V_{\mathrm{pyr}}$ is the energy difference between the localized states $|l^2\rangle$ and $|r^2\rangle$. It thus describes the gain or loss of energy due to the formation of the zwitterionic structures. V_Δ and V_c also interchange their position. V_Δ represents the energy difference between the biradical state $|rl\rangle$ and the average energy of the two zwitterionic states [see Eqs. (8a)–(8c)]. Analogously, V_c gives the energy difference between the $|\pi\pi^*\rangle$ state and the average energy of the $|\pi^2\rangle$ and $|\pi^{*2}\rangle$ states [see Eqs. (7a)–(7c)].

B. Symmetry considerations and two-mode expansion of the potential-energy functions

In principle, the potential matrix is a function of all twelve internal coordinates. As discussed above, only six selected coordinates are considered in the present work: φ, r, ϑ_l, ϑ_r, α_s, and α_a.

In analogy to the *ab initio* surface calculations discussed in Sec. III, the functions $V_{\rm pot}, V_z, V_\pi, V_{\rm pyr}, V_c$, and V_Δ (and thus also the diabatic PE matrices) are represented as restricted two-body expansions,

$$V_i = V_i^{(1D)}(\varphi) + V_i^{(\vartheta_l)}(\varphi,\vartheta_l) + V_i^{(\vartheta_r)}(\varphi,\vartheta_r) + V_i^{(r)}(\varphi,r) + V_i^{(\alpha_s)}(\varphi,\alpha_s) + V_i^{(\alpha_a)}(\varphi,\alpha_a), \tag{9}$$

for $V_i \in \{V_{\rm pot}, V_z, V_\pi, V_{\rm pyr}, V_c, V_\Delta\}$. Except for the torsion φ, the one-body terms are included in $V_i^{(\gamma)}(\varphi,\gamma)$ in this notation. In this expansion, the torsion is pairwise coupled to the other modes, while all other correlation terms have been omitted.

Obviously, all functions have to be 2π-periodic with respect to φ: $V_i^{(\gamma)}(\varphi) = V_i^{(\gamma)}(\varphi + 2\pi)$. Permutation of the two hydrogens at the right CH_2 group transforms $\varphi \to \varphi + \pi$, $\vartheta_r \to -\vartheta_r$ and retains all other coordinate values. This transformation changes the sign of the $|r\rangle$ orbital. Permutation of the two hydrogens at the left CH_2 group analogously transforms $\varphi \to \varphi + \pi$, $\vartheta_l \to -\vartheta_l$ and changes the sign of the $|l\rangle$ orbital. Then from Eq. (8) it follows:

$$V_i(\varphi,\vartheta_r,\vartheta_l) = V_i(\varphi+\pi,-\vartheta_r,\vartheta_l) = V_i(\varphi+\pi,\vartheta_r,-\vartheta_l) \quad \text{for } i \in \{\text{pot},\Delta,\text{pyr},c\}, \tag{10a}$$

$$V_i(\varphi,\vartheta_r,\vartheta_l) = -V_i(\varphi+\pi,-\vartheta_r,\vartheta_l) = -V_i(\varphi+\pi,\vartheta_r,-\vartheta_l) \quad \text{for } i \in \{\pi,z\}. \tag{10b}$$

Since in all terms $V_i^{(\gamma)}$ of the two-body expansion, Eq. (9), either ϑ_l or ϑ_r vanishes, one finds

$$V_i^{(\gamma)}(\varphi,\gamma) = V_i^{(\gamma)}(\varphi+\pi,\gamma) \quad \text{for } i \in \{\text{pot},\Delta,\text{pyr},c\}, \tag{11a}$$

$$V_i^{(\gamma)}(\varphi,\gamma) = -V_i^{(\gamma)}(\varphi+\pi,\gamma) \quad \text{for } i \in \{\pi,z\}. \tag{11b}$$

Combining the above two arguments, one finds that all $V_i^{(\vartheta_l)}(\varphi,\vartheta_l)$ and $V_i^{(\vartheta_r)}(\varphi,\vartheta_r)$ have to be even functions of ϑ_l and ϑ_r, respectively.

There are four permutations which exchange the atoms of the two CH_2 groups. One of these permutations transforms $\varphi \to \varphi$, $\vartheta_r \to \vartheta_l$, $\vartheta_l \to \vartheta_r$, $\alpha_a \to -\alpha_a$ and retains all other coordinate values. This transformation changes the $|r\rangle$-orbital to the $-|l\rangle$-orbital and the $|l\rangle$-orbital to the $-|r\rangle$-orbital. From Eq. (7) follows:

$$V_i(\varphi,\vartheta_l,\vartheta_r,\alpha_a) = V_i(\varphi,\vartheta_r,\vartheta_l,-\alpha_a) \quad \text{for } i \in \{\text{pot},\Delta,\pi,c\}, \tag{12a}$$

$$V_i(\varphi,\vartheta_l,\vartheta_r,\alpha_a) = -V_i(\varphi,\vartheta_r,\vartheta_l,-\alpha_a) \quad \text{for } i \in \{\text{pyr},z\}. \tag{12b}$$

The other three permutations yield equivalent equations. Thus, $V_i^{(\vartheta_r)}$ is completely determined by $V_i^{(\vartheta_l)}$,

$$V_i^{(\vartheta_r)}(\varphi,\vartheta_r) = V_i^{(\vartheta_l)}(\varphi,\vartheta_l) \quad \text{for } i \in \{\text{pot},\Delta,\pi,c\}, \tag{13a}$$

$$V_i^{(\vartheta_r)}(\varphi,\vartheta_r) = -V_i^{(\vartheta_l)}(\varphi,\vartheta_l) \quad \text{for } i \in \{\text{pyr},z\}. \tag{13b}$$

$V_i^{(\alpha_a)}(\varphi,\alpha_a)$ is an even function of α_a for $i \in \{\text{pot},\Delta,\pi,c\}$ and an odd function of the antisymmetric scissor mode for $i \in \{\text{pyr},z\}$.

For further considerations the one-body and two-body terms of expansion (9) are splitted into different classes: $\Gamma_1 = \{1\text{D}, r, \alpha_s\}$, $\Gamma_2 = \{\alpha_a, \vartheta_l, \vartheta_r\}$. Since $V_i^{(\gamma_1)}$ does not depend on ϑ_l, ϑ_r, and α_a for $\gamma_1 \in \Gamma_1$, Eq. (12) yields

$$V_i^{(\gamma_1)}(\varphi,\gamma_1) = -V_i^{(\gamma_1)}(\varphi,\gamma_1) = 0, \quad \text{for } i \in \{\text{pyr},z\}. \tag{14}$$

In D_{2d} symmetry, i.e., for $\varphi = \pi/2$ and any values of r, α_s, the π and π^* orbitals are degenerate. Thus, $V_{\pi^2} = V_{\pi^{*2}}$ in Eq. (7) and $V_\pi^{(\gamma_1)}(\varphi = \pi/2, \gamma_1) = 0$ for $\gamma_1 \in \Gamma_1$. Choosing a diabatic basis where the $|\pi\rangle$ and $|\pi^*\rangle$ orbitals are degenerate for $\varphi = \pi/2$ independent of $\vartheta_l, \vartheta_r, \alpha_a$, one also finds $V_\pi^{(\gamma_2)}(\varphi = \pi/2, \gamma_2) = 0$ for $\gamma_2 \in \Gamma_2$.

In agreement with the symmetry properties discussed above, the functions $V_{\rm pot}^{(\gamma)}$, $V_\Delta^{(\gamma)}$, $V_{\rm pyr}^{(\gamma)}$, $V_c^{(\gamma)}$ will be represented as polynomial expansions in $\sin^2\varphi$ and the functions $V_\pi^{(\gamma)}$ and $V_z^{(\gamma)}$ are given as expansions in $\cos^{2n-1}\varphi$. The functions $V_i^{(\vartheta_l)}, V_i^{(\vartheta_r)}, V_i^{(r)}, V_i^{(\alpha_a)}$, and $V_i^{(\alpha_s)}$ will be given as polynomials in $\vartheta_l^2, \vartheta_r^2, r, \alpha_s$, and α_a, respectively. These functions do not contain purely φ-dependent terms in their polynomial expansions, since the torsional one-body terms are contained in $V_i^{(1D)}$.

C. Analytic representation of the potentials

The expansion coefficients of the PE functions $V_i^{(\gamma)}$ have been determined by a Levenberg–Marquardt least-squares fit procedure using the algorithm provided by the GNU scientific library.[78] Only coefficients which significantly improve the quality of the fit were retained.

The coefficients are determined by a fit of the two lowest adiabatic PE surfaces to the *ab initio* results. The third adiabatic potential energy surface was excluded from the fit, since the quality of the *ab initio* data for the second excited valence-state was significantly lower. Nevertheless the energies predicted by our model for the second excited state surface were checked in regions where the *ab initio* points are considered to be reliable. This comparison provides an additional check of the quality of our model.

The functions $V_i^{(1D)}(\varphi) + V_i^{(\vartheta_l)}(\varphi,\vartheta_l)$, $V_i^{(1D)}(\varphi) + V_i^{(r)}(\varphi,r)$, $V_i^{(1D)}(\varphi) + V_i^{(\alpha_s)}(\varphi,\alpha_s)$, and $V_i^{(1D)}(\varphi) + V_i^{(\alpha_a)}(\varphi,\alpha_a)$, have been determined by separate two-dimensional fits in the respective coordinates. The resulting one-dimensional potentials show the same form,

$$V_{\rm pot}^{(1D)}(\varphi) = A + A_2 \sin^2\varphi + A_4 \sin^4\varphi, \tag{15a}$$

$$V_\pi^{(1D)}(\varphi) = C_1 \cos\varphi + C_3 \cos^3\varphi, \tag{15b}$$

$$V_c^{(1D)}(\varphi) = D, \tag{15c}$$

TABLE III. Parameters of the 2D fit as a function of φ and ϑ. Energies are in eV and angles are in radians.

A	A_2	A_4	A_{02}	A_{04}	A_{22}
6.854	−3.158	1.012	0.5991	0.06073	0.0612
B_{02}	B_{04}	B_{22}			
−0.9895	0.06439	0.1002			
C_1	C_3	C_{12}			
−4.744	−1.533	0.1637			
D	E				
−0.802	1.686				

TABLE V. Parameters of the 2D fit as a function of φ and α_s. Energies are in eV and the angles are in radians.

A	A_2	A_4	A_{0001}	A_{0002}	A_{2001}
6.947	−3.295	1.009	0.458	3.648	0.207
C_1	C_3	C_{1001}	C_{1002}		
−4.767	−1.649	−0.384	0.995		
D	D_{0001}	D_{0002}			
−0.790	−0.177	−0.095			
E	E_{0001}	E_{0002}			
1.600	0.269	−0.709			

$$V_{\Delta}^{(1D)}(\varphi)=E, \tag{15d}$$

$$V_{\mathrm{pyr}}^{(1D)}(\varphi)=0, \tag{15e}$$

$$V_{z}^{(1D)}(\varphi)=0. \tag{15f}$$

The parameter values obtained for $V_i^{(1D)}(\varphi)$ from the different 2D fits were quite similar. For the final results presented, the values from the φ,ϑ_l fit have been chosen.

For $V_i^{(\vartheta_l)}(\varphi,\vartheta_l)$ one obtains

$$V_{\mathrm{pot}}^{(\vartheta_l)}(\varphi,\vartheta_l)=A_{02}\vartheta_l^2+A_{04}\vartheta_l^4+A_{22}(\sin\varphi)^2\vartheta_l^2, \tag{16a}$$

$$V_{\pi}^{(\vartheta_l)}(\varphi,\vartheta_l)=C_{12}(\cos\varphi)\vartheta_l^2, \tag{16b}$$

$$V_{c}^{(\vartheta_l)}(\varphi,\vartheta_l)=0, \tag{16c}$$

$$V_{\Delta}^{(\vartheta_l)}(\varphi,\vartheta_l)=0, \tag{16d}$$

$$V_{\mathrm{pyr}}^{(\vartheta_l)}(\varphi,\vartheta_l)=B_{02}\vartheta_l^2+B_{04}\vartheta_l^4+B_{22}(\sin\varphi)^2\vartheta_l^2, \tag{16e}$$

$$V_{z}^{(\vartheta_l)}(\varphi,\vartheta_l)=0. \tag{16f}$$

The resulting parameters are given in Table III. Figure 5 shows the contour plots of the fitted PES as a function of φ and ϑ in comparison with the *ab initio* results. A detailed discussion will be given in the next section.

The $\varphi-r$ fit results in

$$V_{\mathrm{pot}}^{(r)}(\varphi,r)=A_{001}(r-r^{(0)})+A_{002}(r-r^{(0)})^2+A_{003}(r-r^{(0)})^3+A_{004}(r-r^{(0)})^4+A_{201}(\sin^2\varphi)(r-r^{(0)}), \tag{17a}$$

$$V_{\pi}^{(r)}(\varphi,r)=C_{101}(\cos\varphi)(r-r^{(0)})+C_{102}(\cos\varphi)(r-r^{(0)})^2, \tag{17b}$$

$$V_{c}^{(r)}(\varphi,r)=D_{001}(r-r^{(0)})+D_{002}(r-r^{(0)})^2, \tag{17c}$$

$$V_{\Delta}^{(r)}(\varphi,r)=E_{001}(r-r^{(0)})+E_{002}(r-r^{(0)})^2, \tag{17d}$$

$$V_{\mathrm{pyr}}^{(r)}(\varphi,r)=0, \tag{17e}$$

$$V_{z}^{(r)}(\varphi,r)=0, \tag{17f}$$

where $r^{(0)}$ is the ground-state equilibrium C–C distance. The corresponding parameters are given in Table IV. Contour plots of the adiabatic PE surfaces of the analytical model as function of φ and r are shown in Fig. 6 in comparison to the *ab initio* data.

The fit to $\mathbf{V}^{(1D)}+\mathbf{V}^{(\alpha_s)}$ results in

$$V_{\mathrm{pot}}^{(\alpha_s)}(\varphi,\alpha_s)=A_{0001}\alpha_s+A_{0002}\alpha_s^2+A_{2001}(\sin\varphi)^2\alpha_s, \tag{18a}$$

$$V_{\pi}^{(\alpha_s)}(\varphi,\alpha_s)=C_{1001}(\cos\varphi)\alpha_s+C_{1002}(\cos\varphi)\alpha_s^2, \tag{18b}$$

$$V_{c}^{(\alpha_s)}(\varphi,\alpha_s)=D_{0001}\alpha_s+D_{0002}\alpha_s^2, \tag{18c}$$

$$V_{\Delta}^{(\alpha_s)}(\varphi,\alpha_s)=E_{0001}\alpha_s+E_{0002}\alpha_s^2, \tag{18d}$$

$$V_{\mathrm{pyr}}^{(\alpha_s)}(\varphi,\alpha_s)=0, \tag{18e}$$

$$V_{z}^{(\alpha_s)}(\varphi,\alpha_s)=0. \tag{18f}$$

The parameters for the PE surface as a function of torsion and the symmetric scissor coordinate are summarized in Table V. The adiabatic PE surfaces of the analytic fit are compared with the *ab initio* data in Fig. 7.

TABLE IV. Parameters of the 2D fit as a function of φ and r. Energies are in eV, φ is in radians, and r in atomic units.

A	A_2	A_4	A_{001}	A_{002}	A_{003}	A_{004}	A_{201}
6.868	−3.475	1.280	−4.011	8.6820	−7.75735	3.453231	2.209
C_1	C_3	C_{101}	C_{102}				
−4.512	−1.761	4.393	−0.1373				
D	D_{001}	D_{002}					
−0.878	−0.796	0.2069					
E	E_{001}	E_{002}					
1.611	1.138	−0.2293					

TABLE VI. Parameters of the fit of the antisymmetric scissor coordinate α_a. Energies are in eV, and the antisymmetric scissor angle is in radians.

A_{00002}	4.3823
B_{00001}	0.6416
C_{10002}	0.2589

Due to the problems of the *ab initio* calculations for $\alpha_a \neq 0$ discussed above, $V_i^{(\alpha_a)}$ could not be determined from a straightforward 2D fit in φ and α_a. From the MS-CASPT2 and CASSCF results, the following potentials have been determined (parameter values are given in Table VI),

$$V_{\text{pot}}^{(\alpha_a)}(\varphi,\alpha_a) = A_{00002}\alpha_a^2, \tag{19a}$$

$$V_{\pi}^{(\alpha_a)}(\varphi,\alpha_a) = C_{10002}(\cos\varphi)\alpha_a^2, \tag{19b}$$

$$V_{c}^{(\alpha_a)}(\varphi,\alpha_a) = 0, \tag{19c}$$

$$V_{\Delta}^{(\alpha_a)}(\varphi,\alpha_a) = 0, \tag{19d}$$

$$V_{\text{pyr}}^{(\alpha_a)}(\varphi,\alpha_a) = B_{00001}\alpha_a, \tag{19e}$$

$$V_{z}^{(\alpha_a)}(\varphi,\alpha_a) = 0. \tag{19f}$$

The parameters A_{00002} and C_{10002} have been obtained from a fit to the ground-state MS-CASPT2 results. B_{00001} was determined from the difference of the two upper adiabatic electronic energies for $\varphi = \pi/2$.

D. Discussion of the six-dimensional potential model

The comparison of the global fit to the *ab initio* data in Figs. 5–7 shows that for all cuts the fit of the first two PE surfaces is of good quality. Especially at near-D_{2d} geometries, which are particularly important for the photochemical dynamics, the fit is rather accurate. Although the third state is not included into the fit, its PE surface is predicted in a qualitatively correct manner. The parameters defined in Eq. (15) are determined independently in each 2D fit. The values obtained and reported in Tables III–VI are similar. This again indicates that the electronic-structure model of Sec. IV A describes the essentials of the electronic structure of the valence states of ethene.

Due to its dynamical importance, the φ and ϑ dependence will be investigated more closely. The adiabatic energies of the fitted potential-energy surfaces as well as the *ab initio* data are shown in Fig. 1 as a function of φ. All other coordinates have been fixed at their ground state equilibrium value in Fig. 1(a), while in Fig. 1(b) the C–C distance is 1.486 Å (equilibrium r value of the V state in D_{2h} symmetry). Note that the 2π-periodic diabatic N and Z states cross for $\varphi = \pi/2$ and that the diabatic and adiabatic V states are the same. The adiabatic energies of the second excited state, which have not been explicitly included in the fit, are astonishingly well reproduced.

The adiabatic analytic potentials as a function of the one-sided pyramidalization angle ϑ for perpendicular ethene ($r = 1.486$ Å) are shown in Fig. 3 in comparison to the MS-CASPT2 *ab initio* data. It is seen that the fit is quite accurate near the intersection of the S_0 and S_1 surfaces at $\vartheta \approx 117°$.

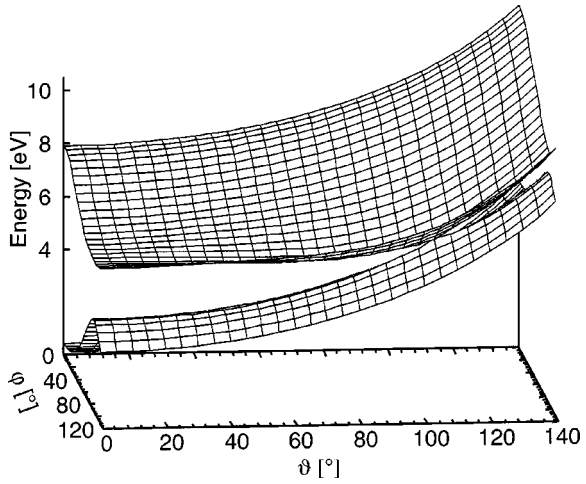

FIG. 9. Conical intersection of the S_0 and S_1 surfaces of ethene in φ,ϑ space. The other coordinates (r,α_s,α_a) have been relaxed to minimize the energy of the intersection.

This is a critical region of the PE surface, since this conical intersection provides the mechanism for ultrafast internal conversion to the electronic ground state. Again, the analytic S_2 PE function agrees fairly well with the *ab initio* data, although these have not been included in the fitting procedure.

The conical intersection of the S_0 and S_1 adiabatic PE surfaces in the φ,ϑ nuclear coordinate space is displayed in Fig. 9. Note that the global surface actually exhibits two of such intersections, corresponding to left or right pyramidalization, respectively. It is seen that the torsion plays the role of the coupling mode: it lifts the accidental degeneracy at $\varphi = 90°$ in first order in the twisting from the perpendicular configuration. Within the 6D analytic PE model, the energy of the point of intersection has been minimized with respect to the remaining coordinates (r,α_s,α_a). The minimum of the seam of intersection is found at $\varphi = 90°$, $\vartheta = 110°$, $\alpha_s = -1°$, $\alpha_a = 1°$, and $r = 1.295$ Å. The energy of the intersection minimum is 6.53 eV, which is 1.42 eV below the vertical excitation energy of the V state.

In the nomenclature of Atchity *et al.*,[79] this conical intersection is of the peaked type in agreement with the findings of Ben-Nun and Martínez.[1] They have found two conical intersections, a peaked intersection as a function of φ and ϑ and a sloped one, which occurs along a hydrogen migration path. The latter is not included in our model, since the CH distances (as well as the rocking coordinates) are frozen.

V. VIBRATIONAL LEVELS

The intention for the development of a three-sheeted six-dimensional PE surface of ethene is the treatment of the photoinduced dynamics in a time-dependent wave packet picture. These calculations will be described in a forthcoming publication.[80] To control some of the approximations invoked in the construction of the surface, in particular the freezing of coordinates and the neglect of intermode coupling terms, it is useful to calculate the lowest vibrational levels of the ground-state surface and to compare these with full-dimensional normal-mode calculations.

TABLE VII. Number of single particle functions (n) and of grid points (N) used for each of the six coordinates. The limiting box (Min, Max) is given in degrees for the angular variables and in Bohr for the stretching coordinate.

Coordinate	n	N	Min	Max
φ	6	96	−90	90
ϑ_l	7	32	−103	103
ϑ_r	7	32	−103	103
α_l	4	32	71	174
α_r	4	32	71	174
r	4	64	−0.8	1.4

We have used the multiconfigurational time-dependent Hartree (MCTDH) method,[81,82] which allows us to deal easily with the six vibrational variables and three electronic states of the problem. In the MCTDH approach, an optimized set of time-dependent basis functions, called single-particle functions, is employed for the description of the wave function. The number of expansion terms required for the representation of the wave function is much smaller than in standard wave packet propagation schemes due to the fact that the uncorrelated motion is represented by the motion of the single-particle functions themselves. The eigenstates are determined via an iterative diagonalization of $\exp(-\beta\mathbf{H})$ based on MCTDH propagation.[83,84] The basis set is defined in Table VII. For all degrees of freedom, a Fourier basis-set representation has been used. 30 Lanczos iterations and $\beta = 400$ a.u. are sufficient to converge the vibrational levels presented. The vibrational levels are computed for the lowest diabatic PE surface as well as for the fully coupled system including all three diabatic potential energy surfaces. The kinetic-energy operator of the system was approximated by neglecting derivative cross terms and terms smaller than m_H/m_C.[80]

Table VIII presents the lowest vibrational levels obtained for the lowest diabatic potential energy surface and for the full model with the three coupled electronic states, respectively, together with the frequencies from *ab initio* harmonic calculations. For all but the symmetric scissor mode, the excitation energies of the fundamentals are lower than the *ab initio* frequencies. The frequency difference between the symmetric and antisymmetric pyramidalization is underestimated by the model. This is a consequence of the fact that the *ab initio* calculations for the construction of the model have been done for one local pyramidalization displacement only, see Sec. IV B. The frequency difference between the two scissor motions is also underestimated. This deficiency is related to the parameters A_{0002} and A_{00002}, which represent the curvature of the PE surface along the symmetric and antisymmetric scissor motions.

TABLE VIII. Comparison of the lowest vibrational energy levels (in cm^{-1}) using the lowest diabatic potential curve (1 state), the full potential model (3 coupled electronic states) and the *ab initio* harmonic frequencies, which were calculated at the MP2 level.

1 state	3 states	Excitation	*Ab initio* (harmonic)
1657	1599	stretch	$\nu_2 = 1684$
1651	1647	2 quanta in pyramidalization	
1649	1636	2 quanta in pyramidalization	
1635	1630	2 quanta in pyramidalization	
1458	1465	antisymmetric scissor	$\nu_6 = 1485$
1448	1453	symmetric scissor	$\nu_3 = 1384$
993	959	torsion	$\nu_4 = 1076$
818	813	symmetric pyramidalization	$\nu_{12} = 984$
816	813	antisymmetric pyramidalization	$\nu_7 = 960$

The calculations performed with the three coupled surfaces correspond to the determination of the vibrational levels of the adiabatic ground-state surface. As one sees in Table VIII, the frequencies for the pyramidalizations and for the scissors are very similar in both cases (diabatic and adiabatic). On the contrary, the frequencies for the torsion and the stretch are both lowered when the three surfaces are taken into account. The fact that the frequency of the torsion is modified is not surprising, since the diabatization along the torsion is important. The change of the frequency for the stretching is directly related to the nonseparability of the potential-energy surface with respect to stretching and torsion.

The vibrational energies presented here are converged to better than $5\ cm^{-1}$ with respect to the MCTDH basis set size. Bearing in mind that the restricted-dimensional analytical potential of the present work has been developed for a description of the three valence electronic states and for large geometry distortions, the agreement between the lowest ground-state vibrational levels and the corresponding full-dimensional *ab initio* frequencies is satisfactory.

VI. CONCLUSIONS

A three-sheeted six-dimensional PE surface of the N, V, and Z valence states of ethene has been constructed on the basis of extended CASSCF/CASPT2 *ab initio* calculations. The six nuclear coordinates, which are considered to be most essential for the UV photochemistry of ethene, are the torsion, the C–C stretch coordinate, the left and right pyramidalization and the symmetric and antisymmetric scissor coordinates. The C–H stretch coordinates and the CH_2 rocking angles, on the other hand, have been frozen at their ground-state equilibrium value. *Ab initio* adiabatic PEs of the N, V, and Z states have been computed as a function of the six selected coordinates, as well as two-dimensional PE cuts, combining the torsion with each of the other five coordinates.

A diabatic representation of the valence states of ethene has been constructed within the framework of a Hückel-type model. A delocalized orbital basis (π, π^*), in which π-binding effects can be described, as well as a localized (p_l, p_r) basis, in which the sudden-polarization effect can be described, are employed. The diabatic PE matrix elements are represented as analytic functions of the relevant nuclear coordinates. The parameters of the analytic functions are determined by a least-squares fit of the eigenvalues of the diabatic PE matrix to the calculated *ab initio* data.

As a function of the torsional coordinate, the analytic PE surface describes the intersection of the V and Z states for torsional angles near 90°. These intersections (four in the interval $0 \leqslant \varphi \leqslant 360°$) are converted into conical intersections in first order of displacements in the antisymmetric

scissor mode. The characterization of these conical intersections is a new result (previous investigators have considered the lifting of the near-degeneracy of the V and Z states of perpendicular ethene by the pyramidalization; this mode, however, can couple the V and Z states only in second order in D_{2d} symmetry).

Another pair of conical intersections, connecting the adiabatic S_1,S_0 or the diabatic N,Z states, arises from the stabilization of the twisted Z state by one-sided (left or right) pyramidalization, as pointed out previously.[1,41,55] The torsional displacement from the perpendicular configuration represents the coupling mode of these conical intersections. It has been shown that the minimum energy of the seam of the S_1-S_0 intersection is energetically accessible after vertical excitation of the V state (near 7.6 eV).

The purpose of the present analytic 6D PE surface is the development of a quantitative time-dependent quantum wave packet description of the internal-conversion process from the photoexcited V state to the electronic ground-state via conical intersections. As a preliminary validation of the reduced-dimensional surface, we have computed in the present work the lowest vibrational levels of the electronic ground state with the MCTDH method and have compared the fundamentals with full-dimensional harmonic vibrational frequencies. A time-dependent wave packet simulation of the photoinduced dynamics of ethene will be reported in a forthcoming publication.

The present PE model for the valence states of ethene can be improved and extended in several ways. Additional nonseparabilities of the six vibrational modes may be taken into account by computing additional two-dimensional cuts (e.g., as a function of C–C stretch and pyramidalization) or by computing selected three-dimensional cuts (e.g., as a function of torsion, C–C stretch and pyramidalization). An extension of the nuclear coordinate space, in particular the inclusion of the C–H stretches to allow for hydrogen migration, also is desirable. In addition, the accuracy of the electronic-structure calculations should be improved by the use of larger basis sets and a more accurate treatment of electron-correlation, e.g., at the MCSCF-MR-CI or MR-AQCC levels.[33] Such calculations are particularly desirable in the vicinity of the conical intersections as a function of the relevant tuning and coupling modes.

We have ignored in the construction of the PE surface the Rydberg excited states of ethene. The PE surfaces of some of these, in particular the $3s$ and $3p$ Rydberg states, intersect the PE surface of the V state, and the consideration of these intersections and their nonadiabatic couplings is essential for a quantitative description of the complex vibronic structure of the UV absorption spectrum of ethene.[10–12,45–49] The $3s$ Rydberg state, in particular, may play an important role in the photochemistry of ethene, leading to excited-state hydrogen detachment processes in competition with internal conversion.[42] The inclusion of the valence-Rydberg conical intersections in the multidimensional PE-surface model of ethene at a high level of electronic-structure theory is another task for future work.

ACKNOWLEDGMENTS

A.V. acknowledges financial support via a Marie Curie fellowship of the European Community program *Improving Human Research Potential and the Socio-Economic Knowledge Base* under Contract No. HPMF-CT-2000-00840. U.M. and W.D. acknowledge financial support by the Deutsche Forschungsgemeinschaft. We thank Wolfgang Eisfeld and Werner Fuß for helpful discussions.

[1] M. Ben-Nun and T. J. Martínez, Chem. Phys. **259**, 237 (2000).
[2] A. J. Merer and R. S. Mulliken, Chem. Rev. **69**, 639 (1969).
[3] M. B. Robin, *Higher Excited States of Polyatomic Molecules* (Academic, New York, 1975), Vol. II.
[4] R. McDiarmid, Adv. Chem. Phys. **110**, 177 (1999).
[5] P. G. Wilkinson and R. S. Mulliken, J. Chem. Phys. **23**, 1895 (1967).
[6] P. D. Foo and K. K. Innes, J. Chem. Phys. **60**, 4582 (1974).
[7] A. J. Merer and R. S. Mulliken, J. Chem. Phys. **50**, 1026 (1969).
[8] R. McDiarmid and E. Charney, J. Chem. Phys. **47**, 1517 (1967).
[9] R. J. Sension and B. S. Hudson, J. Chem. Phys. **90**, 1377 (1989).
[10] J.-S. Ryu and B. S. Hudson, Chem. Phys. Lett. **245**, 448 (1995).
[11] C. Petrongolo, R. J. Buenker, and S. D. Peyerimhoff, J. Chem. Phys. **76**, 3655 (1982).
[12] G. C. Groenenboom, "Novel approaches to the calculation of the electronic structure and dynamics of excited states," Ph.D. thesis, TU Eindhoven, 1991.
[13] P. Farmanara, V. Stert, and W. Radloff, Chem. Phys. Lett. **288**, 518 (1998).
[14] J. M. Mestagh, J. P. Visticot, M. Elhanine, and B. Soep, J. Chem. Phys. **113**, 237 (2000).
[15] R. S. Mulliken, Phys. Rev. **43**, 279 (1933).
[16] L. Salem, *Electrons in Chemical Reactions: First Principles* (Wiley, New York, 1982).
[17] J. Michl and V. Bonačić-Koutecký, *Electronic Aspects of Organic Photochemistry* (Wiley, New York, 1990).
[18] M. Klessinger and J. Michl, *Excited States and Photochemistry of Organic Molecules* (VCH, New York, 1995).
[19] V. Bonačić-Koutecký, P. Bruckmann, P. Hilberty, J. Koutecký, C. Leforestier, and L. Salem, Angew. Chem., Int. Ed. Engl. **14**, 575 (1975).
[20] R. J. Buenker, V. Bonačić-Koutecký, and L. Pogliani, J. Chem. Phys. **73**, 1836 (1980).
[21] L. E. McMurchie and E. R. Davidson, J. Chem. Phys. **67**, 5613 (1977).
[22] B. R. Brooks and H. F. Schaefer III, J. Chem. Phys. **68**, 4839 (1978).
[23] R. J. Buenker, S.-K. Shih, and S. D. Peyerimhoff, Chem. Phys. **36**, 97 (1979).
[24] H. Nakatsuji, J. Chem. Phys. **80**, 3703 (1984).
[25] K. K. Sunil, K. D. Jordan, and R. Shepard, Chem. Phys. **88**, 55 (1984).
[26] R. J. Cave, J. Chem. Phys. **92**, 2450 (1990).
[27] K. B. Wiberg, C. M. Hadad, J. B. Foresman, and W. A. Chupka, J. Phys. Chem. **96**, 10756 (1992).
[28] L. Serrano-Andrés, M. Merchán, I. Nebot-Gil, R. Lindh, and B. O. Roos, J. Chem. Phys. **98**, 3151 (1993).
[29] J. D. Watts, S. R. Gwaltney, and R. J. Bartlett, J. Chem. Phys. **105**, 6979 (1996).
[30] A. M. Mebel, Y.-T. Chen, and S.-H. Lin, J. Chem. Phys. **105**, 9007 (1996).
[31] S. Krebs and R. J. Buenker, J. Chem. Phys. **106**, 7208 (1997).
[32] M. P. Pérez-Casany, I. Nebot-Gil, J. Sánchez-Marín, O. C. Marcos, and J.-P. Malrieu, Chem. Phys. Lett. **295**, 181 (1998).
[33] T. Müller, M. Dallos, and H. Lischka, J. Chem. Phys. **110**, 7176 (1999).
[34] R. J. Buenker, S. D. Peyerimhoff, and S.-K. Shih, Chem. Phys. Lett. **69**, 7 (1980).
[35] R. Lindh and B. O. Roos, Int. J. Quantum Chem. **35**, 813 (1989).
[36] E. R. Davidson, J. Phys. Chem. **100**, 6161 (1996).
[37] M. Persico and V. Bonačić-Koutecký, J. Chem. Phys. **76**, 6018 (1982).
[38] M. Persico, J. Am. Chem. Soc. **102**, 7839 (1980).
[39] G. J. Dormans, G. C. Groenenboom, and H. M. Buck, J. Chem. Phys. **86**, 4895 (1987).
[40] V. Molina, M. Merchán, B. O. Roos, and P.-A. Malmqvist, Phys. Chem. Chem. Phys. **2**, 2211 (2000).
[41] I. Ohmine, J. Chem. Phys. **83**, 2348 (1985).
[42] E. M. Evleth and A. Sevin, J. Am. Chem. Soc. **103**, 7414 (1981).
[43] L. Freund and M. Klessinger, Int. J. Quantum Chem. **70**, 1023 (1998).
[44] A. Warshel and M. Karplus, Chem. Phys. Lett. **17**, 7 (1972).

[45] A. M. Mebel, Y.-T. Chen, and S. H. Lin, Chem. Phys. Lett. **258**, 53 (1996).
[46] A. M. Mebel, M. Hayashi, and S. H. Lin, Chem. Phys. Lett. **274**, 281 (1997).
[47] W. Siebrand, F. Zerbetto, and M. Z. Zgierski, Chem. Phys. Lett. **174**, 119 (1990).
[48] W. Siebrand and M. Z. Zgierski, J. Mol. Struct. **242**, 61 (1991).
[49] J. K. G. Watson, W. Siebrand, M. Pawlikowski, and M. Z. Zgierski, J. Chem. Phys. **105**, 1348 (1996).
[50] V. Sidis, Adv. Chem. Phys. **82**, 73 (1992).
[51] T. Pacher, L. S. Cederbaum, and H. Köppel, Adv. Chem. Phys. **84**, 293 (1993).
[52] W. Domcke and G. Stock, Adv. Chem. Phys. **100**, 1 (1997).
[53] H. Köppel, in *Conical Intersections: Electronic Structure, Dynamics, and Spectroscopy*, edited by W. Domcke, D. R. Yarkony, and H. Köppel (World Scientific, Singapore, 2003).
[54] Z. Liu, L. E. Carter, and E. A. Carter, J. Phys. Chem. **99**, 4355 (1995).
[55] D. Reichhardt, V. Bonačić-Koutecký, P. Fantucci, and J. Jellinek, Chem. Phys. Lett. **279**, 129 (1997).
[56] M. Ben-Nun, J. Quenneville, and T. J. Martínez, J. Phys. Chem. A **104**, 5161 (2000).
[57] T. Vreven, F. Bernardi, M. Garavelli, M. Olivucci, M. A. Robb, and H. B. Schlegel, J. Am. Chem. Soc. **119**, 12687 (1997).
[58] M. Ben-Nun and T. J. Martínez, Chem. Phys. Lett. **298**, 57 (1998).
[59] J. C. Tully, J. Chem. Phys. **93**, 1061 (1990).
[60] G. Granucci, M. Persico, and A. Toniolo, J. Chem. Phys. **114**, 10608 (2001).
[61] G. Stock, J. Chem. Phys. **103**, 1561 (1995).
[62] M. Ben-Nun and T. J. Martínez, J. Phys. Chem. A **103**, 10517 (1999).
[63] B. O. Roos, Adv. Chem. Phys. **69**, 399 (1987).
[64] K. Andersson and B. O. Roos, in *Modern Electronic Structure Theory*, edited by D. R. Yarkony (World Scientific, Singapore, 1995), Vol. 1, pp. 55–109.
[65] M. J. Frisch, G. W. Trucks, H. B. Schlegel *et al.*, GAUSSIAN 98, Revision A.9, Gaussian, Inc., Pittsburgh, PA, 1998.
[66] T. H. Dunning, J. Chem. Phys. **90**, 1007 (1989).
[67] J. Finley, P.-A. Malmqvist, B. O. Roos, and L. Serrano-Andrés, Chem. Phys. Lett. **288**, 299 (1998).
[68] K. Andersson, M. Barysz, A. Bernhardsson *et al.*, MOLCAS, Version 5.2 (University of Lund, Sweden, 2001).
[69] L. S. Bartell, E. A. Roth, C. D. Hollowell, K. Kuchitsu, and J. E. Young, J. Chem. Phys. **42**, 2683 (1965).
[70] K. Kuchitsu, J. Chem. Phys. **44**, 906 (1966).
[71] J. M. L. Martin, T. J. Lee, P. R. Taylor, and J.-P. Francois, J. Chem. Phys. **103**, 2589 (1995).
[72] A. M. Ahern, R. L. Garrell, and K. D. Jordan, J. Phys. Chem. **92**, 6228 (1988).
[73] D. Van Lerberghe, I. J. Wright, and J. L. Duncan, J. Mol. Spectrosc. **42**, 251 (1972).
[74] J. L. Duncan and E. Hamilton, J. Mol. Spectrosc. **76**, 65 (1981).
[75] H. Köppel, W. Domcke, and L. S. Cederbaum, Adv. Chem. Phys. **57**, 59 (1984).
[76] H. Köppel and W. Domcke, in *Encyclopedia of Computational Chemistry*, edited by R. von Rague-Schleyer (Wiley, New York, 1998), p. 3166.
[77] J. Tennyson and J. N. Murrell, Nouv. J. Chim. **5**, 361 (1981).
[78] M. Galassi, J. Davies, J. Theiler, B. Gough, R. Priedhorsky, G. Jungman, M. Booth, and F. Rossi, GNU Scientific Library: http://www.gnu.org/software/gsl/ (2001).
[79] G. J. Atchity, S. S. Xantheas, and K. Ruedenberg, J. Chem. Phys. **95**, 1862 (1991).
[80] A. Viel, R. P. Krawczyk, U. Manthe, and W. Domcke (unpublished).
[81] H.-D. Meyer, U. Manthe, and L. S. Cederbaum, Chem. Phys. Lett. **165**, 73 (1990).
[82] U. Manthe, H. D. Meyer, and L. S. Cederbaum, J. Chem. Phys. **97**, 3199 (1992).
[83] T. Gerdts and U. Manthe, J. Chem. Phys. **107**, 6584 (1997).
[84] U. Manthe and F. Matzkies, Chem. Phys. Lett. **252**, 71 (1996).